Materials Research Bulletin 171 (2024) 112636

Contents lists available at ScienceDirect

Materials Research Bulletin

journal homepage: www.elsevier.com/locate/matresbu

Research Papers

Switchable phase transitions from non-magnetic to magnetic cerium oxide nanoparticles using acoustic shock waves

Sivakumar Aswathappa [a], Lidong Dai [a,*], Sahaya Jude Dhas Sathiyadhas [b], Martin Britto Dhas Sathiyadhas Amalapushpam [c], Mowlika Varadhappa [d], Raju Suresh Kumar [e], Abdulrahman I. Almansour [e]

[a] Key Laboratory of High-temperature and High-pressure Study of the Earth's Interior, Institute of Geochemistry, Chinese Academy of Sciences, Guiyang, Guizhou 550081, China
[b] Department of Physics, Kings Engineering College, Sriperumbudur, Chennai, Tamilnadu 602 117, India
[c] Shock Wave Research Laboratory, Department of Physics, Abdul Kalam Research Center, Sacred Heart College, Tirupattur, Tamil Nadu 635 601, India
[d] Department of Physics, St Joseph's College of Arts and Science for Women, Hosur Krishnagiri, Tamilnadu 635 126, India
[e] Department of Chemistry, College of Science, King Saud University, P.O. Box 2455, Riyadh 11451, Saudi Arabia

ARTICLE INFO

Keywords:
Magnetic state transitions
Shock waves
CeO_2 NPs
Spin-split band transition

ABSTRACT

In the present framework, we report a reversible magnetic phase transition that occurs from a mixed diamagnetic (nonmagnetic) state to a weak ferromagnetic (magnetic) state exhibited by cerium oxide nanoparticles (CeO_2 NPs) under shocked conditions wherein the magnetic phase transitions are observed to be switchable phase transitions of mixed diamagnetic - weak ferromagnetic - mixed diamagnetic - weak ferromagnetic for the respective shock pulses of 0, 50, 100 and 150, which is probably reported for the first time, and the observed values of the saturation magnetization are 0.9117, 0.1022, 0.8783 and 3.7780 emu/g, respectively. The possible reasons behind the observed reversible magnetic phase transition are proposed by the outcomes attained from the spectroscopic and microscopic techniques. Based on the obtained analytical results, it is confirmed that the observed room temperature weak ferromagnetism is because of the enhancement of Ce^{3+} ions (reduction of Ce^{4+} ions) and oxygen vacancies such that the title material is suggested for the applications of magnetic sensors.

1. Introduction

Considering the popular classes of materials that are compatible with the development of advanced technology, materials with a blend of nanocrystalline magnetic nature could contribute a great deal of resounding success whereby various research teams pioneer to scale up the process of making those materials. On the extent of these counts, searching for ferromagnetism that exists in technologically important oxide nanocrystalline materials such as TiO_2, ZnO, and CeO_2 has a long track record over the past few years due to their spectacular progress in the field of making magnetic devices. Note that, theoretically, the nanomaterials of TiO_2, ZnO, and CeO_2 belong to the diamagnetic state because of their outermost electronic configuration [1,2]. Researchers have observed a weak ferromagnetic state in the above-mentioned nanomaterials at room temperature due to the formation of oxygen vacancies during the process of synthesis [3–7]. Special mention is that the formation of oxygen vacancies in the crystal lattice plays an imperative role whereby an efficient differentiation is created in the magnetic state of the materials (especially metal oxides) and numerous research work has been carried out on this topic which brings about several controversial results, whereas a proper authentication on the formation of ferromagnetic state out of the diamagnetic state of materials is yet to be arrived at [8,9]. To fix these indistinct scientific issues, the intended prevailing experiments on the magnetic properties of diamagnetic nano-crystalline materials are in full swing, especially for chemical dopants at high-temperature, low-temperature and high-pressure techniques.

As witnessed, over a century, a series of techniques such as static high-pressure (DAC) [10,11], static temperature [12,13], high power laser irradiation [14], high energy gamma-ray irradiation [15], very high energy ion bombardment [16], electron bombardment [17], laser shock wave [18,19], and acoustical shock waves [20,21] have been employed to explore deeply the physical and chemical properties of materials under extreme environmental conditions. Among the

* Corresponding author.
E-mail address: dailidong@vip.gyig.ac.cn (L. Dai).

https://doi.org/10.1016/j.materresbull.2023.112636
Received 2 September 2023; Received in revised form 14 November 2023; Accepted 24 November 2023
Available online 25 November 2023

above-mentioned techniques, exposing the test material to acoustic shock waves is one of the crucial techniques that could establish a great deal of innovative findings. Shock waves can be generated by a well-equipped shock tube of tabletop nature which requires a small research laboratory that is affordable. After the invention of the tabletop shock tubes (Reddy Tube) [22,23], the applications of shock waves in the materials science branch have attained the stature of being one of the outstanding succinct research topics such that numerous spectacular results have been found in variety of aspects such as reversible and irreversible crystal to crystal phase transition [24,25] reversible and irreversible crystal to amorphous and vice versa [26,27] while in a few other cases, reversible and irreversible molecular phase transitions and magnetic phase transitions have been witnessed [28,29]. Note that, even though most of the materials undergo structural transitions and deformations, a few materials are highly stable under shocked conditions [30–34]. Among the above-mentioned types of phase transitions under shocked conditions, the shock wave-induced switchable phase transitions are quite interesting as there is no crystal-clear science available at this point on the switchability of materials which are yet to be explored to the extent that is required thereby relevant and feasible mechanism could be arrived at. Materials with the ability of switchable phase transitions can be utilized for applications in thermo-nuclear devices, magnetic sensors, phase shifters, accelerate meters, pressure transmitters and current flash memories [32,34].

In recent years, the crystallographic structural stability of a few metallic oxide nanoparticles such as ZnO, ZrO_2, TiO_2 and Co_3O_4 has been examined and arrived at spectacular results in terms of crystallographic as well as magnetic phase transitions [28,35-39]. Following these metal oxides, our research group has examined the crystallographic phase stability of CeO_2 NPs under acoustical shocked conditions and found a stable crystallographic phase which has been confirmed by the conventional powder X-ray diffraction profiles and Raman spectroscopic results [40]. Based on the fruitful implications of the prominent findings [41], it is a way forward to repeat the experiment and perform similar acoustic shock wave loading procedures with the same Mach number (2.2) to understand the nature of magnetic and electrical transport properties of CeO_2 NPs. Because the literature survey shows that a variety of complex results are probable in the magnetic properties of CeO_2 NPs. With respect to the theoretical aspects and as per the electronic configuration, the chemical specimen of CeO_2 is in a diamagnetic state due to the unavailability of unpaired electrons in the outermost shell [41,42]. The integrative action of ions such as Ce_{4f} and O_{2p} makes the CeO_2 nonmagnetic. However several nanoscience researchers have found weak ferromagnetism in their respective CeO_2 NPs [43] and the occurrence of weak ferromagnetism is because of the formation of oxygen deficiency in the surface (in most of the cases) and oxygen vacancies in the bulk crystal structure (reduction of the Ce^{4+}) such that a few reports are listed [44,45]. Note that ferromagnetism is relatively uncommon in oxide materials (ZnO, TiO2, CeO_2, HfO_2, In_2O_3) except in major oxide families such as hexa-ferrites, garnets, spinels, and mixed-valence perovskites structures [44]. The experimental findings of the room temperature weak ferromagnetism in CeO_2 have been reported by several groups worldwide [46–51]. Very recently, one of the papers has appeared in the journal of *Nat. Phys* which accounts for the possible evidence of the ferromagnetic state in CeO_2 NPs caused by the influence of spin-orbit coupling concepts [52]. Following this article, the same research group has published a review article based on the room temperature magnetism in CeO_2 wherein the authors have cited nearly 150 articles for the room temperature magnetic state of the CeO_2 NPs whereas, no paper has come up with the information on the actual diamagnetic or mixed diamagnetic states [53]. The magnetic behaviour of CeO_2 NPs under shocked conditions is yet to be reported.

In the present research work, the switchable magnetic phase transition occurring from mixed diamagnetic state to weak ferromagnetic state is demonstrated with respect to the number of shock pulses, and to the best of our understanding, this is the first report as of now on the conversion from diamagnetic state to weak ferromagnetic state wherein neither any change in the crystallographic aspects nor total chemistry of the test sample is witnessed.

2. Experimental procedure

The experimental procedure of the synthesis of CeO_2 NPs and the details of the shock tube, as well as the shock wave loading process are provided in the supplementary section. In Fig. 1, the schematic diagram of the tabletop pressure-driven shock tube and the observed magnetic transitions occurring in the Cubic CeO_2 NPs are presented. The required shock waves are generated by an in-house semiautomatic Reddy Tube which is capable of producing supersonic shock waves. It has three sections such as driver, driven and diaphragm sections. The driver and driven sections are made of seamless steel tubes of length 48 cm and 33 cm, respectively and both have the same inner diameter of 1.5 cm. Atmospheric air is used as the working substance for the required shock wave generation which is supplied by a tabletop mini 1 HP air compressor that has the capacity of 8 bars of pressure storage. The diaphragm section separates the driver section and the driven section. Carbonless paper diaphragms are fed into the diaphragm section with the help of a motor. While the atmospheric air is being compressed into the driver section, at the critical pressure, the diaphragm is ruptured such that the shock wave is generated and moves along the driven section. In the present experiment, shock waves of Mach number 2.2 have been utilized possessing the dynamic transient pressure of 2 MPa and temperature 864 K.

3. Results and discussion

3.1. Magnetic properties

The understanding of the room temperature magnetic properties of CeO_2 NPs continues to be not in the clear spectrum such that the experimentalists as well as the theoretical researchers go on with consistent effort to tackle it. On those count, we have provided the observed results which are based on the experimental concepts of ferromagnetism in CeO_2 [52,53]. In the present case, a vibrating sample magnetometer (VSM) has been utilized to verify the magnetic state of the control and acoustic shock wave-treated CeO_2 NPs whereby the obtained room temperature M-H loops are shown in Fig. 2 wherein the control sample of CeO_2 NPs exhibit a mixed nonmagnetic phase (very low magnetic field-super-paramagnetic state and high magnetic field-diamagnetic state) and based on the control sample' M-H loop, it is clear that the most of the loop area covered is in the diamagnetic state and such kind of mixed diamagnetic state of CeO_2 NPs is very rare in the literature [41–53]. In the case of the control CeO_2 NPs, the formation of the mixed diamagnetic state clearly represents that the concentration of Ce^{4+} ions is very high whereas a very small amount of oxygen vacancies and Ce^{3+} ions are present in the crystal lattice and because of these facts; a low magnetic field is maintained in the title sample such that it exhibits room temperature weak ferromagnetic behaviour. If the crystal lattice is free of Ce^{3+} ions and oxygen vacancies it would be a perfect diamagnetic state. Due to the nature of the synthesis process carried out, the formation of oxygen vacancies has been quite uncontrollable [41–53].

Surprisingly, at the 50-shocked condition, the formation of the room temperature weak ferromagnetic state is ensured in the NPs because of very low coercivity and low saturation magnetization whereas at the 100-shocked condition, again it reverts to the mixed diamagnetic state as in the case of the control sample. On further increasing the shock number to 150, it turns back to the weak ferromagnetic state such that this kind of magnetic switchable phase transitions from a nonmagnetic to a magnetic state has never been reported to date. While increasing the number of shock pulses, the degree of recrystallization and surface modification keep on varying which results in different aspects of outcomes for the different number of shock pulses and also it can vary with

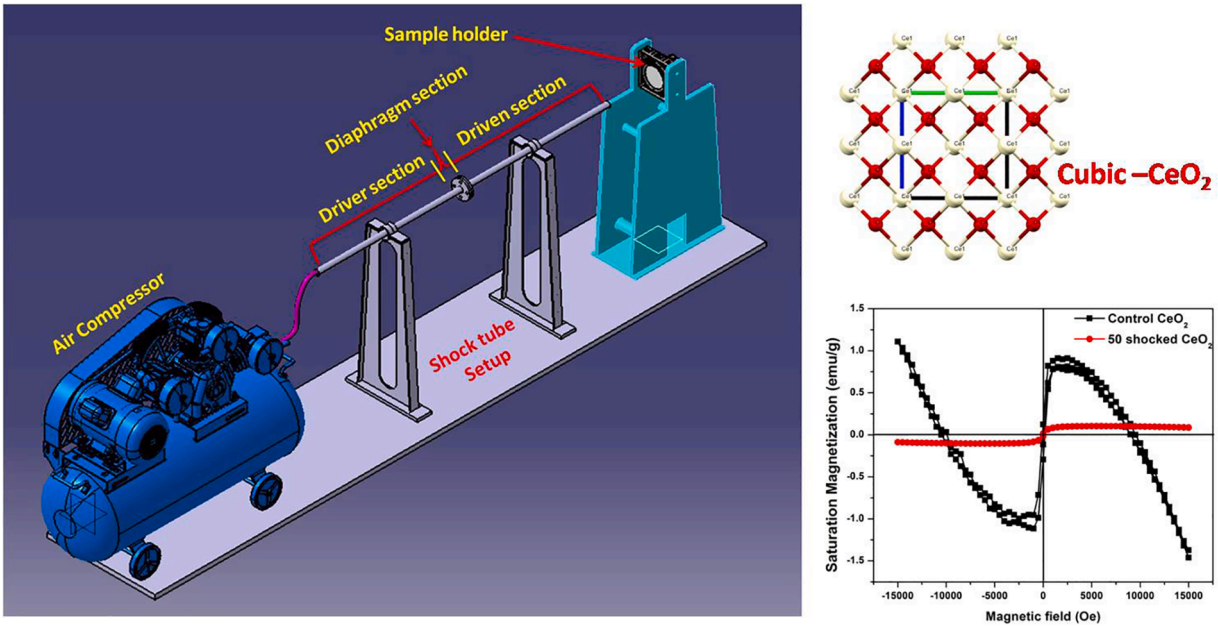

Fig. 1. Schematic diagram of the tabletop pressure driven shcok tube and the magantic transtions occuring in the cubic CeO_2 NPs.

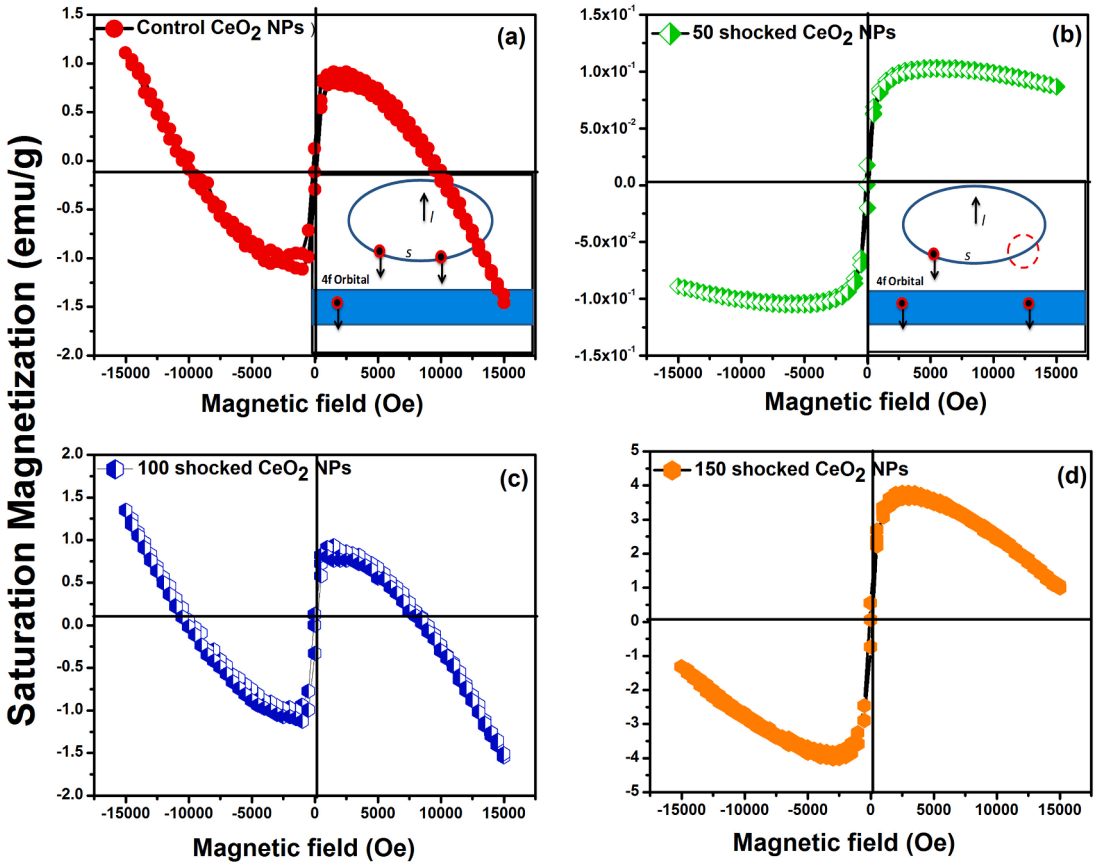

Fig. 2. M-H loops of the control and acoustical shock wave-treated cerium oxide NPs (a) control (b) 50 (c)100 and (d)150 shocked CeO_2 NPs.

respect to the nature of the target materials. Such kind of shock wave-induced switchable transitions are quite known [24,27,28]. The saturation magnetization values of the control, 50,100 and 150 shock pulses are 0.9117, 0.1022, 0.8783 and 3.7780 emu/g, respectively. In general nano-synthesis processes, such kind of room temperature weak ferromagnetic state usually occurs in the case of CeO_2 NPs which may not be new [45–53]. But, in the present case, the synthesized CeO_2 NPs are nearly in the mixed diamagnetic state which in turn becomes a ferromagnetic state thereby it could be treated as a remarkable result of magnetic state transition occurring under shocked conditions. Because of the existing facts, it is very difficult to achieve magnetic phase transitions under acoustic shock wave-treated conditions wherein no change

occurs either in the original crystallographic structure or in the shape of the particles. Herewith, a few of the examples for the above-mentioned claims are listed based on the previously reported articles. Very recently, Arijit Roy *et al.*, have reported the shock wave-induced transformation of a non-magnetic to a magnetic state of the ISM dust of ferrocinece (Iron and cyclopentadiene). Note that, as per the observed results under shocked conditions, the ferrocinece has been converted into α-Fe and Fe_3C materials and obviously they are highly magnetic materials [54]. Mowlika *et al.*, have reported the ferromagnetic to super-paramagnetic state of $CoFe_2O_4$ NPs due to the occurrence of significant lattice distortions under shocked conditions [55]. But, in the present case, there is neither significant crystallographic change nor particle shape change occurring under shocked conditions [40]. Hence, more insights are solicited for the mechanism responsible for the appearance of the room temperature weak ferromagnetic state of CeO_2 NPs under 50 and 150 shocked conditions. The interesting aspect of the attainment of room-temperature ferromagnetic state in CeO_2 NPs leads to two prominent questions i.e. (i) How can be a magnetic state traced for mixed diamagnetic materials such as CeO_2 NPs? (ii) Why does it not turn into a perfect diamagnetic state instead of a weak ferromagnetic state? In this context, it is worthwhile to bring in a few spin-splitting concepts to justify the occurrence of the room-temperature ferromagnetic state in CeO_2. Note that CeO_2 is extensively used as a catalyst because of its ability to switch its average oxidation states in a suitable temperature range without undergoing any structural changes [52,53] which clearly represents that the oxidation states of CeO_2 are highly temperature as well as pressure sensitive. Moreover, when the external temperature or pressure is changed there could be changes in the oxidation states and number of coordination bonds [11,28,29]. Because of magnetic state changes, it is not merely an intrinsic property governed by atomic-scale defects within the particles. The topology of the surface of contiguous particles is also a critical factor. As mentioned previously, stoichiometric cerium oxide exhibits a diamagnetic nature because of the Ce^{4+} ions that occupy the completely filled shell. When the shock wave pressure is applied on the sample, some of the Ce^{4+} ions are turned into Ce^{3+} ions due to the changes which are due to the reduction of Ce^{4+} ion into Ce^{3+} ion thereby leading to non-stoichiometry such that defects are introduced into the CeO_2 crystal lattice to compensate the charge and the resultant spin coupling with the nearest-neighbor interaction by double exchange (Ce^{3+}–O–Ce^{4+}) by charge transfer transition occurring between O_{2p} and Ce 4f energy bands. Due to the shock wave-induced reduction process of Ce^{4+} ions, a quite high concentration of Ce^{3+} ions may lead to a greater number of oxygen vacancies in the sample. Note that the magnetic moments of cerium, oxygen and oxygen vacancies are 4 μB, 2 μB and 1.2 μB, respectively. Due to the high value of magnetic moment for the oxygen vacancies, they play a significant role in contributing to the magnetic properties. In addition to that, generally, the electrons are strongly associated with defects in oxides which have a high dielectric constant and thereby occupy a large number of Bohr orbitals that tend to form an impurity band where they may experience localized potential fluctuations in the crystal lattice. In such cases, by allowing the impurity band to mix with the 4f states of cerium (please see the insets in Fig. 2) and transferring one electron for each vacancy, the 4f states would in turn polarize the impurity band and provide the necessary ferromagnetic coupling in the CeO_2 for which the detailed mechanism of the formation of ferromagnetism is presented in Fig. 3. In the literature, it is found that the weak paramagnetic CeO_2 is converted into the ferromagnetic state when the samples are irradiated with 200 MeV swift heavy Xe ions irradiation fluence of 2×10^{13} ions/cm^2 [56]. But, in the present case, just 2.0 MPa shock pressure could trigger the same phase transition which indicates that the magnetic state of CeO_2 NPs is highly sensitive to the shock transit temperature and pressure. One can see the perfect structure of a tetrahedral CeO_2 supercell with 32 cerium atoms and 64 oxygen atoms. Each oxygen atom is surrounded by four cerium atoms at the same distance. From the total DOS of CeO_2, all the electron spin-up and spin-down states are symmetric and show no magnetism in the perfect CeO_2 cell. Fig. 3 represents the schematic of super-exchange interaction among 1Ce, 2Ce, and O atoms when two Ce atoms are reduced by two electrons based on the formation of oxygen vacancy thereby forming a Ce–O–Ce bond along with the neighboring O atom which favors a 90-degree super-exchange interaction such that it leads to the magnetism in CeO_2 [52,53,57,58]. Fig. 3 b-f clearly represents the step-by-step process of the super-exchange interaction of Ce–O–Ce. Initially, one electron of one O_{2p} orbital is excited by the applied shock pressure whereby one 4f orbital of 1 Ce atom (Fig. 3c) and the excited electron spin direction become parallel to the electron of Ce 4f orbital based on Hund's rule (Fig. 3d) [52,53,57,58]. Since the Ce–O–Ce bond angle is close to 90 °, the electron with the same spin direction to another O 2p orbital is exchanged with 4f orbital of 2 Ce atom (Fig. 3e) which makes the spin direction of the electron of 2 Ce 4f orbital parallel to it (Fig. 3f) thereby the resultant direction of magnetic moments of these two Ce atoms become the same such that it leads to the ferromagnetic coupling in the crystal lattice. Meanwhile, at the bottom of the conduction band, O 2p exhibits slight asymmetry which contributes to the formation of the conduction band of CeO_2. With one oxygen vacancy, the calculated magnetism of the sample is about 1.213

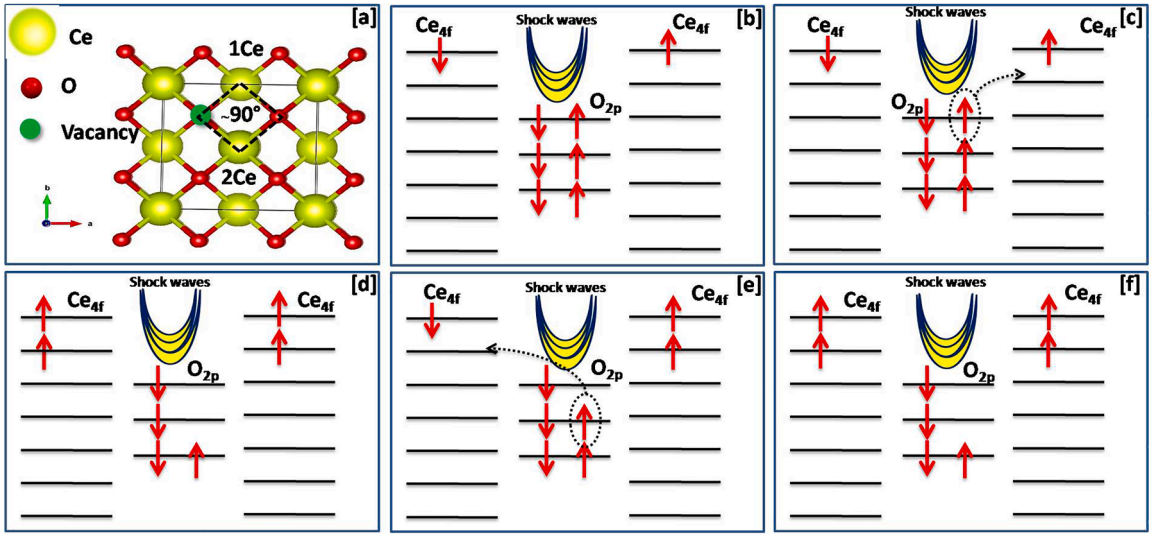

Fig. 3. Possible mechanism for the conversion of diamagnetic to ferromagnetic state of CeO_2 under shocked conditions.

μB. After another oxygen atom is removed, two oxygen vacancies are formed [58]. With the increase in oxygen vacancies, the tetrahedral structure of the sample is further destroyed to make the Ce atoms close to the oxygen vacancies, which increases the total magnetic momentum. As shock wave transient pressure-temperature produces more oxygen vacancies in the structure of CeO_2, the electron spin on Ce 4f orbitals becomes more complicated such that it makes the projected density of states of Ce 4f more asymmetric [58]. Thus, shock wave impact can enhance magnetism by producing oxygen vacancies.

At the exposure of 100 to 150 shock pulses, the density of the defects and oxygen vacancy are considerably increased whereby a weak ferromagnetic state may exist. On that count, it becomes apparent that a weak ferromagnetic state may occur at the exposure of 120 shocks because of the formation of defects. To examine this probability, VSM analysis for the 120 shocked CeO_2 sample has been performed and the obtained M-H loop is presented in Fig. 4. As seen in Fig. 1, the mixed diamagnetic state is converted into the room temperature weak ferromagnetic state at the 120-shocked condition and the calculated value of saturation magnetization is 0.25 emu/g. Note that the value of lower saturation magnetization clearly represents the defect density which is quite lower than that of the 150-shocked condition.

Therefore, based on the overall observation, it could be taken into account that while under shocked conditions, some of the Ce^{4+} ions experience the reduction and are converted into Ce^{3+} ions thereby it may bring the room temperature weak ferromagnetic state in CeO_2. Moreover, the reflections of spectroscopic and microscopic analyses could provide evidence for the spin splitting and the formation of defective crystal structure at the 50-shocked condition which can further be revealed by the implementation of XPS and TEM studies that appear in the upcoming sections.

3.2. X-ray photoelectron spectroscopy study

The XPS study could provide further details on the valence state changes (even a very small quantity in atomic ratio) and surface atomic compositions of the test samples. Hence, X-ray Photoelectron Spectroscopic study (PHI - VERSAPROBE III – X-ray Photoelectron Spectroscopy) has been performed for CeO_2 samples to confirm the mixed diamagnetic to ferromagnetic phase transition occurring at the 50-shocked condition and the observed XPS survey spectra of the control and 50 shocked CeO_2 samples are shown in Fig. 5 and peak shift profiles are presented in Fig. 6

As seen in Fig. 6a, the survey XPS spectra of the control sample are found to be well-matched with the previous reports [57–59] and the sample of 50 shocked doesn't show any significant change while looking

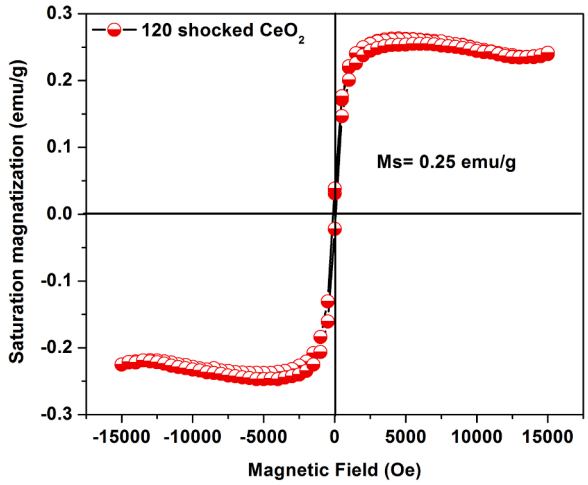

Fig. 4. M-H loop of the 120 shocked cerium oxide NPs.

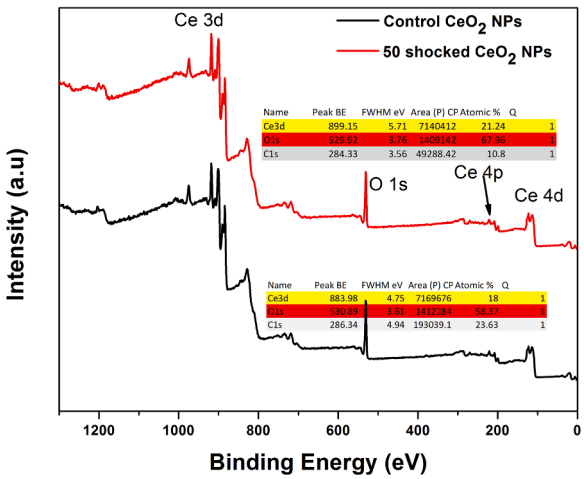

Fig. 5. XPS survey spectra of control and 50 shocked CeO_2 NPs samples.

through the naked eye. But, while looking at the zoomed-in version of the 3d core level spectra, it could be observed a lower binding energy shift for the sample of 50 shocked which provides considerable evidence for the formation of the defective crystal structure along with the oxygen vacancies [57–59]. In the control sample, the XPS bands appear at 975.01, 918.215, 909.062 (Ce^{3+}), and 900.549 eV which belong to the $Ce3d_{5/2}$ while the other XPS bands appear at 889.885 (Ce^{4+}) and 884.027 eV and these belong to the $Ce3d_{3/2}$. Fig. 6b clearly represents that all the bands experience the lower binding energy shift at the 50-shocked condition.

The bonding present between cerium and oxide is covalent which involves hybridization of the 4f (Ce) orbitals of Ce^{4+} cations and the filled 2p (O) orbitals of the O^{2-} anions. Each Ce^{4+} cation is coordinated by eight equivalent O^{2-} anions positioned at the corners of the cube, and each O^{2-} is coordinated in turn by a tetrahedron of Ce^{4+} ions. Note that the Ce^{4+} ion has a closed shell [Xe] $4f^15d^16s^2$ configuration with no unpaired electrons. Based on Fig. 6b, the attained lower binding energy shift for the 50-shocked sample confirms that the coordination number decreases from eight and moves towards the lower number of coordination bonds which enhances the formation of Ce^{3+} ions in the crystal lattice. Note that the observed binding energy shift is also related to the removal of O atoms from the regular sites thereby, if one oxygen atom is removed from the lattice, two oxygen vacancies are formed such that the resultant net magnetic moment would increase. In such cases, the net atomic percentage of the Ce and O atoms can be shown with some considerable changes under shocked conditions and the reduction in the O atomic percentage is expected because of the formation of the oxygen vacancies. To extract such crucial information, the deconvoluted core-XPS spectra of the Ce 3d and O1 s spectra are presented in Fig. 7 for the control and 50 shocked samples.

Note that, in the case of the control sample (Fig. 7a), the Ce^{4+} XPS peak is located at 918.215 eV whereas at the 50-shocked condition (Fig. 7b), it got shifted towards the lower binding energy side (towards the Ce^{3+}) and it is probably because of the reduction in the number of Ce^{4+} ions in the 50-shocked CeO_2 crystalline lattice. The observed results can also declare that the valence band is formed mostly of O 2p states whereas the conduction band is composed mainly by Ce 4f and Ce 5d states hence, the electronic transport properties are significantly altered which could be correlated with the EIS spectroscopic analysis.

For the control sample, O 1 s spectra can be fitted into two distinct peaks which are generally represented as $O_{lattice}$ (O_L) and $O_{surface}$ (Os) which are located at 529.69 eV and 531.31 eV, respectively (Fig. 7c). At the 50-shocked condition, the O_L and Os peaks got higher binding energy shift and are located at 529.76 eV and 531.23 eV (Fig. 7d). As can be seen in Fig. 7 (c and d), the shape of the O 1 s spectra is not much changed whereas, the value of full width at half maximum has

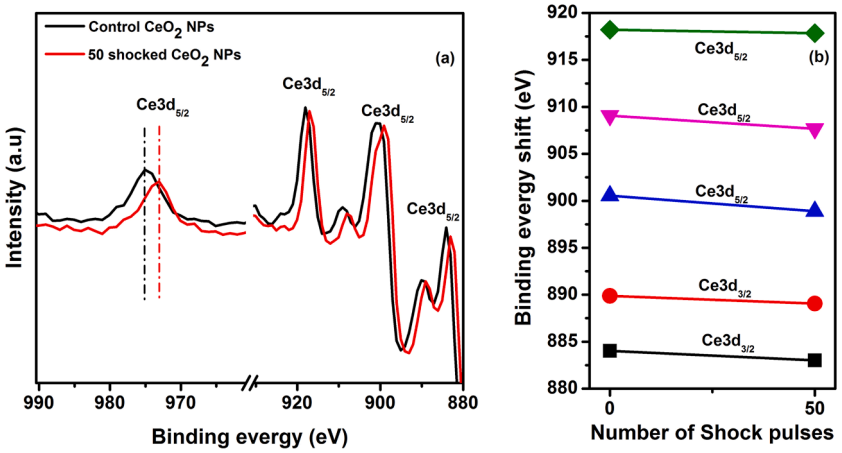

Fig. 6. XPS peak shift profiles of the control and 50 shocked CeO_2 NPs.

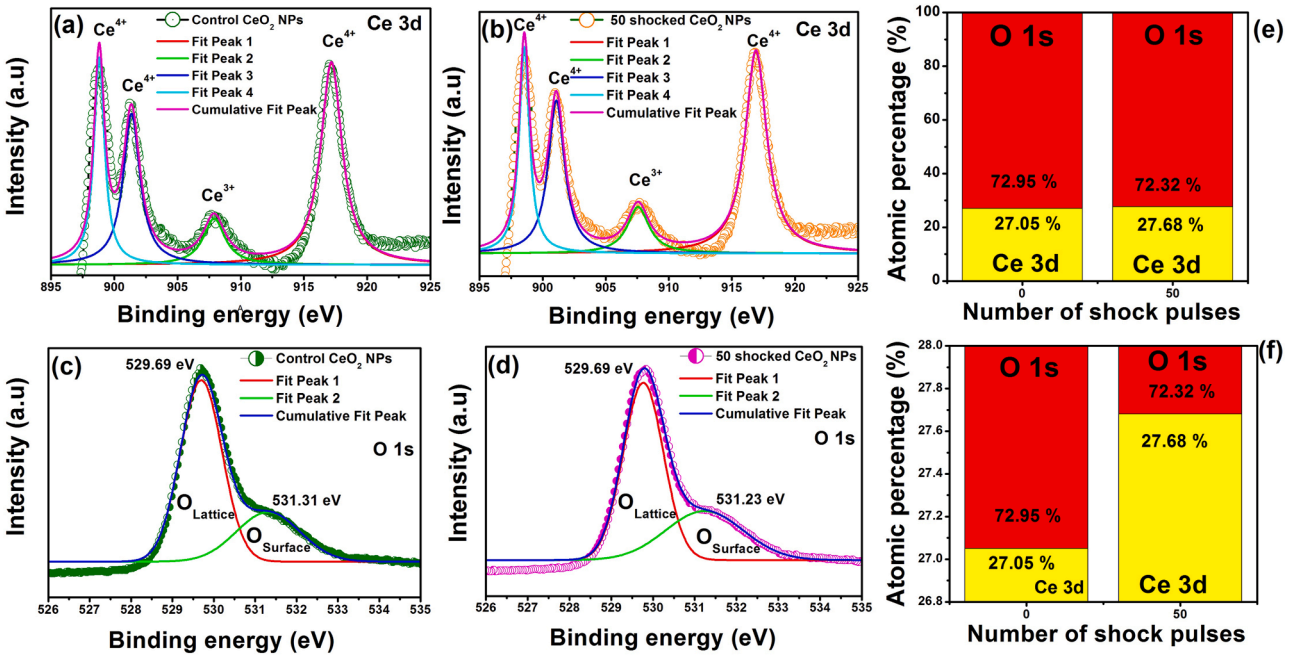

Fig. 7. Core XPS spectral features of the control and 50 shocked samples (a) core Ce 3d spectra of the control sample (b) core Ce 3d spectra of the shocked CeO_2 NPs (c) core O 1 s spectra of the control sample (d) core O 1 s spectra of the shocked CeO_2 NPs, (e and f) atomic percentages of the Ce and O atoms for the control and 50-shocked condition.

considerably decreased for the O_L at the 50-shocked condition compared to the control sample and it is also found a slight enhancement of the Os peak's full width at half maximum. As per the observed core-XPS Ce and O band spectral analysis, the calculated Ce and O atomic percentages are 27.05 and 72.95 % for the control sample while 27.68 and 72.32 % for the 50-shocked sample such that the corresponding figures are presented in Fig. 7 (e and f). As per the observed values of the atomic ratio percentages, it is clear that the Ce^{3+}/Ce^{4+} ratio is slightly enhanced compared to the control sample and in contrast, O atomic ratio percentages are found to have reduced. The enhancement of the Ce^{3+}/Ce^{4+} ratio at the 50-shocked condition is probability due to the enhancement of the Ce^{3+} ions in the crystalline lattice followed by the formation of oxygen vacancies [57–59]. Moreover, while there is an increase in the number of Ce^{3+} ions in the crystal system, the unit cell volume may expand. Because, the radius of Ce^{3+} ions is quite higher than Ce^{4+} ions such that the values are found to be 0.1283 nm and 0.1098 nm, respectively. In addition to that, according to Fig. 7, the Ce^{4+} core-XPS spectra of the control and 50-shocked CeO_2 samples as well as the observed results of Ce^{4+} core spectra well support the intended consideration. Based on the XPS study, it is quite clear that the formation of more Ce^{3+} ions and oxygen vaccines are the major contributors to have induced the room temperature weak ferromagnetic state in 50-shocked CeO_2 NPs while in the present case, Ce^{3+} ions provide the superior contribution compared to the oxygen vaccines.

3.3. *Transmission electron microscopic study*

Transmission Electron Microscopic (TEM) analysis could be used to extract the local atomic disorders such as surface defects, atomic defects (vacancies), etc in the nano-sized materials. Moreover, TEM results can provide robust shreds of evidence for the understanding of the formation of ferromagnetic state under 50 and 150 shocked conditions such that the TEM measurements have been performed for the control, 50, 100 and 150 shocked samples thereby the captured surface images and Morrie lattice fringe patterns are presented in Fig. 8. Here, the particles in the (111) plane are strongly considered for the understanding of the

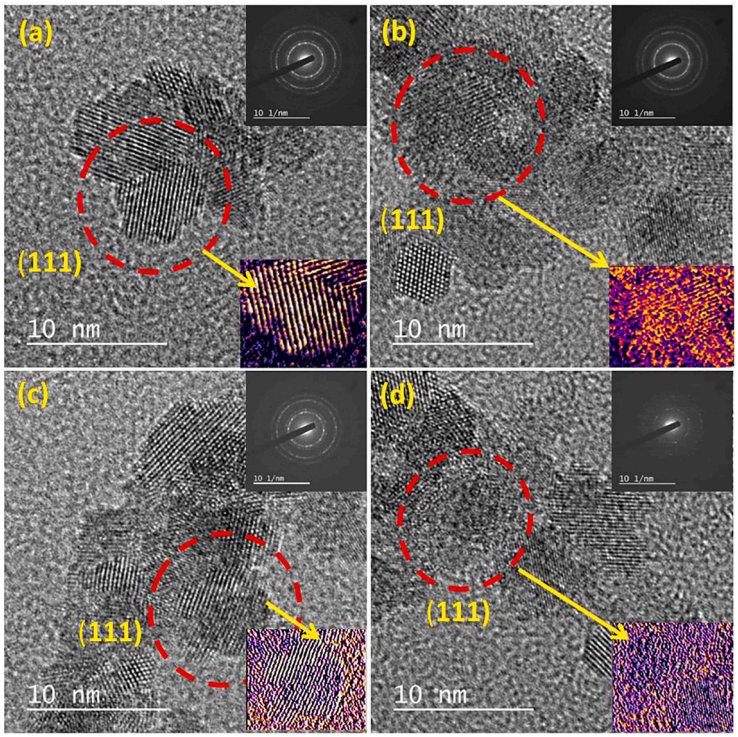

Fig. 8. TEM images of (a) the control CeO_2 (b) 50-shocked CeO_2 (c) 100-shocked CeO_2 and (d) 100-shocked CeO_2 NPs (Note: Insets in top right selected area are electron diffraction (SAED) patterns of CeO_2 and insets in the bottom right selected area are zoomed-in portions).

atomic disorder in the crystal lattice. Because the spherical and nano-octahedra-shaped particles of the (111) plane are more favorable than those of the (001) and (110) for the formation of oxygen vacancies [53]. Note that the surface/volume ratio of the nanoparticles decreases when the ionic radius increases. In the present case also, it could be expected that the surface/volume ratio is decreased because of the presence of a greater number of Ce^{3+} ions in the 50-shocked sample which leads to a high number of unsaturated Ce–O bonds on the surface and such kind of bonds play a significant part in the transport properties such as optical, electrical and thermal properties.

As seen in Fig. 8a, the particles of the control sample are crystallized in a spherical shape for which the average grain size is 6 nm. The highly ordered Morrie fringe pattern and SAED pattern of the control sample are presented in Fig. 8a as insets. As seen in Fig. 8a, the bright dots in the SAED pattern and in the zoomed-in portion of the Morrie fringe pattern clearly represent the local atomic lattice order of the control CeO_2 which is very high. Whereas, in the 50-shocked sample, the surface morphology (Fig. 7b) is found to have undergone slight changes. Moreover, while looking at the SAED pattern and Morrie lattice fringe patterns (Fig. 8b), a lot of inter-atomic defects are observed such that these results could evidently justify the formation of surface defects. Notably, at the 50-shocked condition, the intensities of higher-order diffraction ring patterns are slightly reduced compared to the control sample which may be because of the formation of defects in the crystalline lattice. At 100-shocked condition, the defect density in the surface as well as crystalline lattice is considerably reduced which may be due to the shock wave-induced dynamic recrystallization [24,25] and the captured TEM image and SAED pattern are presented in Fig. 8c. As seen in Fig. 8c, the observed SAED pattern and Morrie fringe patterns are found to be quite similar to the control sample which clearly emphasize that the density of the defects are considerably reduced at the 100-shocked condition that can be one of the prime reasons for the conversion of weak ferromagnetic to mixed diamagnetic state (Fig. 2). More interestingly, the significant changes could be seen in the local atomic structure of CeO_2 NPs at the 150-shocked condition compared to the other shocked conditions and the captured TEM image and SAED patterns are presented in Fig. 8d. As reflected in Fig. 8d, the formation highly defective grains could be witnessed and the SAED patterns show a significant reduction of intensity in the higher angle diffraction lines. In SAED patterns, the ring intensities are directly proportional to the degree of crystalline nature where higher spot intensity indicates a high degree of crystallinity. In this context, it is worth noting that the 150-shocked sample has high-level defects in the crystalline lattice and this defect density may be the reason for the observation of high saturation magnetization. Based on the observed features of SAED and Morrie fringe patterns of the 50 and 150 shocked samples, it is quite clear that the 150-shocked sample has a high concentration of defects compared to the 50-shocked sample which may lead to the formation of a weak ferromagnetic state with higher saturation magnetization. The calculated average particle size of the control, 50, 100, and 150 shocked samples are 6 nm (± 1 nm), 8 nm (± 1 nm), 7 (± 1.2 nm), and 9 nm (± 1.5 nm), respectively. Considering the particle size of the control and shocked samples, an increase of 3 nm is observed for the 150-shocked CeO_2 sample which may be due to the formation of more Ce^{3+} ions in the defective crystal lattice. As discussed earlier, Ce^{3+} ions (0.1283 nm) have a higher atomic radius than that of Ce^{4+} (0.1098 nm) and at the 150-shocked condition, the particle size is increased because of the higher atomic radius of Ce^{3+} ions.

3.4. *Electrochemical impedance spectroscopic results*

The appearance of changes in valance bands such as Ce^{3+} and Ce^{4+} might have significantly altered the electronic transport properties so that the electrochemical impedance spectroscopic study has been undertaken for the control and shocked samples and the Cole-Cole plots are drawn utilizing the observed data as presented in Fig. 9. Based on the obtained Nyquist plots of the control and shocked samples, the existence of the incomplete semicircular arcs (asymmetric arcs) confirms the existence of the non-Debye type of relaxation type CeO_2 which is found to be well-matched with the previous results [60]. However, while looking

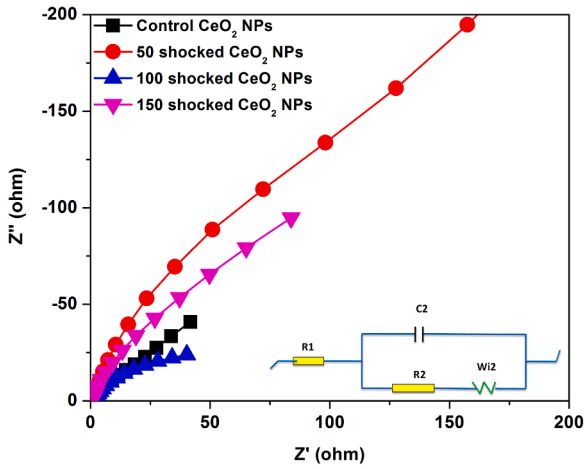

Fig. 9,. Nyquist plots of the control, 50, 100 and 150 shocked CeO_2 NPs.

at the arc width of the control and shocked samples, there is a resemblance of switchable phase transitions with respect to the number of shock pulses as reflected in the magnetic properties. Based on the obtained plots, it is clear that the control and 100 shocked samples have higher electrical conductivity whereas 50 and 150 shocked samples have comparatively lower electrical conductivity. On the other hand, the control and 100 shocked samples possess lower impedance values (lower dielectric constant) whereas 50 and 150 shocked samples have higher impedance values (higher dielectric constant) such that the reasons behind these changes could be as follows. With reference to the previous sections, the ionic radius of Ce^{3+} is quite high compared to the Ce^{4+} ions which lead to the lattice expansion along with the formation of oxygen vacancies and such multiple oxygen vacancies have highly probable tendency to align along the ⟨111⟩ directions.

Generally, such kind of reduction of the valence band induces (more Ce^{3+} ions in the crystal) an increase in the lattice constant which enforces a significant decrease in electrostatic forces for the nearest atoms in the crystal system whereby the net electrical conductivity of the NPs is reduced under 50 and 150 shocked conditions [61,62]. In addition, the formation of oxygen vacancies in CeO_2 not only contributes to the increment of the lattice constant but also significantly contributes to the increase in the mutual repulsion of Ce cations near the sites of oxygen vacancies and because of these factors the net electrical conductivity is reduced for the NPs under 50 and 150 shocked conditions. Note that, according to the literature, most of the non-stoichiometry oxides exhibit insulating behaviour (low electrical conductivity) [52,53]. As per the local spin density approximation GGA calculation aspect, when an oxygen atom is removed from a perfect CeO_2 crystal lattice, it will introduce the electrons directly into the narrow 4f band which spontaneously splits to form a half-metallic nature from the metallic nature thereby it reduces the nature of conductivity [53]. Moreover, while increasing the oxygen vacancies i.e. when oxygen is removed, the electrons left behind not only localize the Ce 4f orbitals but also the vacant oxygen site itself leading to the spin polarization and ferromagnetic super-exchange and it indicates the formation of defective crystal structure of CeO_2. The reduction of Ce atoms not only populates the Ce^{3+} ions but also induces the displacement of the sub-lattice oxygen plane system hence electron scattering process is more predominant in the defective crystal structure [53,61,62]. In Fig. 10, the real and imaginary parts of the impedance spectra of the control and shocked CeO_2 NPs are shown. As reflected in both the cases of Fig. 10 (a and b), the control and 100 shocked CeO_2 NPs have almost similar values whereas, 50 and 150 shocked CeO_2 NPs possess higher values thereby the trend of these values are found to be well-matched with the observed magnetic properties. While comparing to the 50-shocked sample's real part of impedance, the 150-shocked sample CeO_2 has a slightly lower real and imaginary part of the impedance which may be because of the formation of more oxygen vacancies, surface defects in the crystalline lattice and such vacancies and defects facilitate the observed electrical transportation [63,64].

Conclusion

Based on the observed magnetic, spectroscopic and electron microscopic results on the control and shocked CeO_2 NPs, the following interpretations are consolidated. Cubic cerium oxide NPs undergo switchable mixed diamagnetic to ferromagnetic phase transition against the number of shock pulses such as 0, 50, 100 and 150 shocked conditions. The formation of the room temperature weak ferromagnetism at the 50-shocked condition could be explained by the spin-split band approaching concepts as well as XPS spectroscopic results which are well-supported by the spin-splitting band concepts. TEM results also provide convincing evidence for the highly defective crystal structure and the formation of oxygen vacancies at the 150-shocked condition as against the control sample and other shocked conditions which lead to the higher saturation magnetization. EIS spectroscopic results could effectively converge all the observed magnetic, spectroscopic and electron microscopic implications in such a way that it could be blended into a single point whereby the weak ferromagnetic CeO_2 samples have a relatively lower electrical conductivity. This kind of novel switchable magnetic state materials can provide unique insights that would pave the way for the design of new spintronics devices and the applications of magnetic sensors.

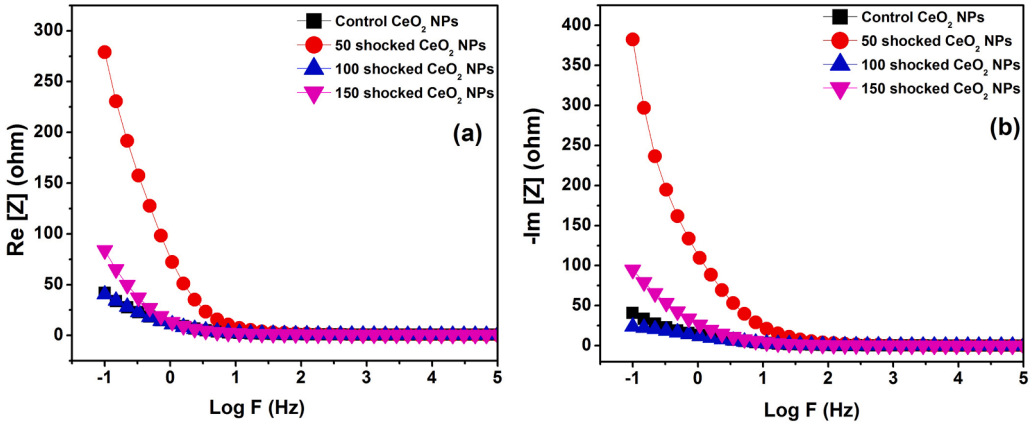

Fig. 10,. (a) The real and (b) the imaginary part of the impedance spectra of the control and shocked CeO_2 NPs.

Ethics approval

Not applicable.

Consent to participate

All the authors agree to participate.

Informed consent

All people involved in or responsible for the research are informed and consent.

Compliance with ethical standards

None.

Availability of data

The data that support the findings of this study are available from the corresponding author upon reasonable request.

CRedit authorship contribution statement

Sivakumar Aswathappa and Lidong Dai: Data analysis, Investigation, Writing-original draft; **Sahaya Jude Dhas Sathiyadhas**: Visualization, Roles/Writing - original draft; **Martin Britto Dhas Sathiyadhas Amalapushpam**: Visualization, Writing-review & editing, **Mowlika Varadhappa Reddy:** Formal Analysis and sample preparation, **Raju Suresh Kumar**: Formal Analysis, **Abdulrahman I. Almansour**- Formal Analysis.

Declaration of Competing Interest

The authors declare that they have no conflict of interest.

Data availability

Data will be made available on request.

Acknowledgment

The authors thank NSF of China (42072055). The project was supported by Researchers Supporting Project number (RSP2023R142), King Saud University, Riyadh, Saudi Arabia.

Supplementary materials

Supplementary material associated with this article can be found, in the online version, at doi:10.1016/j.materresbull.2023.112636.

References

[1] Parmanand Sharma, Amita Gupta, K.V. Rao, Frank J. Owens, Renu Sharma, Rajeev Ahuja, J.M. Osorio Guillen, Börje Johansson, G.A. Gehring, Ferromagnetism above room temperature in bulk and transparent thin films of Mn-doped ZnO, Nat. Mater. 2 (2003) 673–677.

[2] Yuji Matsumoto, Makoto Murakami, Tomoji Shono, Tetsuya Hasegawa, Tomoteru Fukumura, Masashi Kawasaki, Parhat Ahmet, Toyohiro Chikyow, Shin-Ya Koshihara, Hideomi Koinuma, Room-temperature ferromagnetism in transparent transition metal-doped titanium dioxide, Science 291 (2001) 854.

[3] H. Ohno, Making nonmagnetic semiconductors ferromagnetic, Science 281 (1998) 951–956.

[4] Walid Sharmoukh, Talaat A. Hameed, Saad Mabrouk Yakout, New nonmagnetic aliovalent dopants (Li^{+}, Cu^{2+}, In^{3+} and Ti^{4+}): Optical and strong intrinsic room temperature ferromagnetism of perovskite $BaSnO_3$, J. Alloy. Compound. 925 (2022), 166702.

[5] Li-Ting Tseng, Xi Luo, Sean Li, Jiabao Yi, Magnetic properties of Sm-doped rutile TiO_2 nanorods, J. Alloy. Compound. 687 (2016) 294–299.

[6] A.N. Morozovska, E.A. Eliseev, M.D. Glinchuk, R. Blinc, Surface-induced magnetism of the solids with impurities and vacancies, Physica B 406 (2011) 1673–1688.

[7] Erika Tothova, Mamoru Senna, Anatoly Yermakov, Jozef Kovac, Erika Dutkova, Michal Hegedus, Maria Kanuchova, Matej Balaz, Zdenka Lukacova Bujnakova, Jaroslav Briancin, Petre Makreski, Zn source-dependent magnetic properties of undoped ZnO nanoparticles from mechanochemically derived hydrozincite, J. Alloy. Compound. 787 (2019) 1249–1259.

[8] Yue Kang, Qiang Leng, Donglin Guo, Dezhi Yang, Yanping Pu, Chenguo Hu, Room-temperature magnetism of ceria nanocubes by inductively transferring electrons to ce atoms from nearby oxygen vacancy, Nano. Micro. Lett. 8 (2016) 13–19.

[9] G. Jayakumar, A. Albert Irudayaraj, A. Dhayal Raj, S. John Sundaram, K. Kaviyarasu, Electrical and magnetic properties of nanostructured Ni doped CeO_2 for optoelectronic applications, J. Phys. Chem. Solids. 160 (2022), 110369.

[10] Xiaoli Huang, Defang Duan, Kai Wang, Xinyi Yang, Shuqing Jiang, Wenbo Li, Fangfei Li, Qiang Zhou, Xilian Jin, Bo Zou, Bingbing Liu, Tian Cui, Structural and electronic changes of $SnBr_4$ under high pressure, J. Phys. Chem. C. 117 (2013) 8381–8387.

[11] Quanjun Li, Bingbing Liu, Lin Wang, Dongmei Li, Ran Liu, Bo Zou, Tian Cui, Guangtian Zou, Yue Meng, Ho-kwang Mao, et al., Pressure-induced morphization and polyamorphism in one-dimensional single-crystal TiO_2 nanomaterials, J. Phys. Chem. Lett. 1 (2010) 309–314.

[12] Yun-Zhi Tang, Yin-mei Yu, Jian-bo Xiong, Yu-Hui Tan, He-Rui Wen, Unusual high temperature reversible phase transition behavior, structures and dielectric-ferroelectric properties of two new crown ether clathrates, J. Am. Chem. Soc. 137 (2015) 13345–13351.

[13] Yun-Zhi Tang, Yi Liu, Ji-Xing Gao, Chang-Feng Wang, Bin Wang, Yu-Hui Tan, He-Rui Wen, Reversible structural phase transition, ferroelectric and switchable dielectric properties of an adduct molecule of hexamethylenetetramine ferrocene carboxylic acid, RSC Adv 7 (2017) 41369.

[14] Xiao Dong, Ning Li, Zhen Zhu, Hezhu Shao, Ximing Rong, Cong Liang, Haibin Sun, Guojin Feng, Li Zhao, Jun Zhuang, A nitrogen-hyperdoped silicon material formed by femtosecond laser irradiation, Appl. Phys. Lett. 104 (2014), 091907.

[15] M.A. Ahlam, M.N. Ravishankar, N. Vijaya, G. Govindaraj, A.P.Gnana Prakash Siddaramaiah, Investigation of gamma radiation effect on chemical properties and surface morphology of some nonlinear optical (NLO) single crystals, Nuc. Inst. Meth. Phys. Res B. 278 (2012) 26–33.

[16] A.V. Krasheninnikov, K. Nordlund, Ion and electron irradiation-induced effects in nanostructured materials, J. Appl. Phys. 107 (2010), 071301.

[17] F. Pesty, P. Garoche, Low-energy electron beam on an insulator surface: Impact of the charging process on the diffraction by mica muscovite, Sur. Sci. 580 (2005) 153–162.

[18] Zhi Su, William L. Shaw, Yu-Run Miao, Sizhu You, Dana D. Dlott, Kenneth S. Suslick, Shock wave chemistry in a metal−organic framework, J. Am. Chem. Soc. 139 (2017) 4619–4622.

[19] Xuan Zhou, Yu-Run Miao, William L. Shaw, Kenneth S. Suslick, Dana D. Dlott, Shock wave energy absorption in metal−organic framework, J. Am. Chem. Soc. 141 (2019) 2220–2223.

[20] V. Jayaram, A. Gupta, K.P.J. Reddy, Investigation of strong shock wave interactions with CeO_2 ceramic, J. Adv. Ceram. 3 (2014) 297–305.

[21] K. Vasu, H.S.S.R. Matte, Sharmil N. Shirodkar, V. Jayaram, K.P.J. Reddy, Umesh V. Waghmare, C.N.R. Rao, Effect of high-temperature shock-wave compression on few-layer MoS_2, WS_2 and $MoSe_2$, Chem. Phys. Lett. 582 (2013) 105–109.

[22] K.P.J. Reddy, N. Sharath, Manually operated piston-driven shock tube, Curr. Sci 104 (2013) 172–175.

[23] A. Sivakumar, S. Balachandar, S.A. Martin Britto Dhas, Measurement of "shock wave parameters" in a novel table-top shock tube using microphones, Human. Fact. Mech. Eng. Defen. Safty. 4 (2020) 3.

[24] A. Sivakumar, S. Reena Devi, S. Sahaya Jude Dhas, R. Mohan Kumar, K. Kamala Bharathi, S.A. Martin Britto Dhas, Switchable phase transformation (orthorhombic−hexagonal) of potassium sulfate single crystal at ambient temperature by shock waves, Cryst. Growth. Des. 20 (2020) 7111–7119.

[25] V. Jayaram, P. Singh, K.P.J. Reddy, Experimental investigation of nano ceramic material interaction with high enthalpy argon under shock dynamic loading, Appl. Mech. Mater. 83 (2011) 66–72.

[26] V. Jayaram, G. Bowtham, Experimental investigation of oxidation resistance of SiC powder for the protection of re-entry space vehicle using material shock tube, Adv. Matter. Lett. 9 (2018) 510–515.

[27] A. Sivakumar, S. Sahaya Jude Dhas, J. Thirupathy, K.P.J. Reddy, Raju Suresh Kumar, Abdulrahman I. Almansour, Shubhadip Chakraborty, S.A. Martin Britto Dhas, Switchable crystal–amorphous states of $NiSO_4{\cdot}6H_2O$ induced by a Reddy tube, New. J. Chem. 46 (2022) 5091.

[28] A. Sivakumar, A. Rita, S. Sahaya Jude Dhas, K.P.J. Reddy, Raju Suresh Kumar, Abdulrahman I. Almansour, Shubhadip Chakraborty, K. Moovendaran, Jayavel Sridhar, S.A. Martin Britto Dhas, Dynamic shock wave driven simultaneous crystallographic and molecular switching between α-Fe_2O_3 and Fe_3O_4 nanoparticles – a new finding, Dalton. Trans. 51 (2022) 9159–9166.

[29] A. Sivakumar, S. Soundarya, S. Sahaya Jude Dhas, K.Kamala Bharathi, S.A. Martin Britto Dhas, Shock wave driven solid state phase transformation of Co_3O_4 to CoO nanoparticles, J. Phys. Chem. C. 124 (2020) 10755–10763.

[30] N. Koteeswara Reddy, V. Jayaram, E. Arunan, Y.B. Kwon, W.J. Moon, K.P.J. Reddy, Investigations on high enthalpy shock wave exposed graphitic carbon nanoparticles, Diamond. Rel. Mater. 35 (2013) 53–57.

[31] A. Sivakumar, S. Sahaya Jude Dhas, Abdulrahman I. Almansour, Raju Suresh Kumar, Natarajan Arumugam, S.A. Martin Britto Dhas, Spectroscopic assessment of shock wave resistance on zno nanorods for aerospace applications, J. Inorg. Organomet. Polym. 31 (2021) 2553–2559.
[32] A. Sivakumar, S. Sahaya Jude Dhas, Shubhadip Chakraborty, Raju Suresh Kumar, Abdulrahman I. Almansour, Natarajan Arumugam, S.A. Martin Britto Dhas, Dynamic shock wave-induced amorphous-to-crystalline switchable phase transition of lithium sulfate, J. Phys. Chem. C. 126 (2022) 3194–3201.
[33] Kosuke Usui, Mikinori Ando, Daisuke Yokogawa, Stephan Irle, Understanding the on−off switching mechanism in cationic tetravalent group-v-based fluoride molecular sensors using orbital analysis, J. Phys. Chem. A. 119 (2015) 12693–12698.
[34] Noelia Fuentes, Ana Martin-Lasanta, Luis Alvarez de Cienfuegos, Maria Ribagorda, Andres Parra, Juan M. Cuerva, Organic-based molecular switches for molecular electronics, Nanoscale 3 (2011) 4003.
[35] V. Jayaram, Preetam Singh, K.P.J. Reddy, Study of anatase TiO_2 in the presence of N_2 under shock dynamic loading in a free piston driven shock tube, Adv. Ceram. Sci. Eng. 2 (2013) 41–46.
[36] S. Kalaiarasi, A. Sivakumar, S.A. Martin Britto Dhas, M. Jose, Shock wave induced anatase to rutile TiO_2 phase transition using pressure driven shock tube, Mater. Lett. 219 (2018) 72–75.
[37] M. Devika, N. Koteeswara Reddy, V. Jayaram, K.P.J. Reddy, Sustainability of aligned ZnO nanorods under dynamic shock-waves, Adv. Mater. Lett. 8 (2017) 398–403.
[38] V. Jayaram, K.P.J. Reddy, Experimental study of the effect of strong shock heated test gases with cubic zirconia, Adv. Mater. Lett. 7 (2016) 100–150.
[39] A. Sivakumar, S. Kalaiarasi, S. Sahaya Jude Dhas, P. Sivaprakash, S. Arumugam, M. Jose, S.A. Martin Britto Dhas, Comparative assessment of crystallographic phase stability of anatase and rutile TiO_2 at dynamic shock wave loaded conditions, J. Inorg. Organomet. Polym 32 (2022) 967–972.
[40] A. Sivakumar, S. Ramya, S. Sahaya Jude Dhas, Abdulrahman I. Almansour, Raju Suresh Kumar, Natarajan Arumugam, Magesh Murugesan, S.A. Martin Britto Dhas, Assessment of crystallographic and electronic phase stability of shock wave loaded cubic cerium oxide nanoparticles, Ceram. Inter. 48 (2022) 1963–1968.
[41] Rafael Schmitt, Andreas Nenning, Olga Kraynis, Roman Korobko, Anatoly I. Frenkel, Igor Lubomirsky, Sossina M. Hailef, Jennifer L.M. Rupp, A review of defect structure and chemistry in ceria and its solid solutions, Chem. Soc. Rev. 49 (2020) 554–592.
[42] V. Fernandes, P. Schio, A.J.A de Oliveira, W.A Ortiz, P. Fichtner, L. Amaral, I. L Graff, J. Varalda, N. Mattoso, W.H. Schreiner, D.H. Mosca, Ferromagnetism induced by oxygen and cerium vacancies above the percolation limit in CeO_2, J. Phys.: Condens. Matter. 22 (2010), 216004.
[43] Norge C. Hernandez, Ricardo Grau-Crespo, Nora H.de Leeuw, Javier Fdez Sanz, Electronic charge transfer between ceria surfaces and gold adatoms: a GGA+U investigation, Phys. Chem. Chem. Phys. 11 (2009) 5246–5252.
[44] K. Shimizu, S. Kosugi, Y. Tahara, K. Yasunaga, Y. Kaneta, N. Ishikawa, F. Hori, T. Matsui, A. Iwase, Change in magnetic properties induced by swift heavy ion irradiation in CeO_2, Nuc. Inst. Method. Phys. Res B. 286 (2012) 291–294.
[45] M. Venkatesan, C.B. Fitzgerald, J.M.D. Coey, Unexpected magnetism in a dielectric oxide, Nature 430 (2004) 630.
[46] A. Sundaresan, R. Bhargavi, N. Rangarajan, U. Siddesh, C. Rao, Ferromagnetism as a universal feature of nanoparticles of the otherwise nonmagnetic oxides, Phys. Rev. B. 74 (2006), 161306.
[47] Shih-Yun Chen, Yi-Hsing Lu, Tzu-Wen Huang, Der-Chung Yan, Chung-Li Dong, Oxygen vacancy dependent magnetism of CeO_2 nanoparticles prepared by thermal decomposition method, J. Phys. Chem. C. 114 (2010) 19576–19581.
[48] V. Fernandes, R.J.O. Mossanek, P. Schio, J.J. Klein, A.J.A. de Oliveira, W.A. Rtiz, N. Mattoso, J. Varalda, W.H. Schreiner, M. Abbate, D.H. Mosca, Dilute-defect magnetism: Origin of magnetism in nanocrystalline CeO_2, Phy. Rev. B. 80 (2009), 035202.
[49] Shalendra Kumar, Young Joo Kim, B.H. Koo, Chan Gyu Lee, Structural and magnetic properties of Ni doped CeO_2 nanoparticles, J. Nanosci. Nanotechnol. 10 (2010) 7204–7207.
[50] Sumeet Kumar, Manish Srivastava, Jay Singh, Samar Layek, Madhu Yashpal, Arnulf Materny, Animesh K. Ojha, Controlled synthesis and magnetic properties of monodispersed ceria nanoparticles, AIP Adv. 5 (2015), 027109.
[51] M. Li, R. Zhang, H. Zhang, W. Feng, X. Liu, Synthesis, structural and magnetic properties of CeO_2 nanoparticles, Micro. Nano. Lett. 5 (2010) 95–99.
[52] Michael Coey, Karl Ackland, Munuswamy Venkatesan, Siddhartha Sen, Collective magnetic response of CeO_2 nanoparticles, Nat. Phys. 12 (2016) 694–699.
[53] Karl Ackland, J.M.D. Coey, Room temperature magnetism in CeO_2—a review, Phys. Rep. 746 (2018) 1–39.
[54] Arijit Roy, Surendra V. Singh, J.K. Meka, R. Ramachandran, D. Sahu, A. Gautam, T. Vijay, Jayaram Vishakantaiah, P. Janardhan, B.N. Rajasekhar, Anil Bhardwaj, N. J. Mason, B. Sivaraman, Shock-induced transformation of non-magnetic to magnetic ISM dust analogue, MNRAS 517 (2022) 4845–4855.
[55] V. Mowlika, C.S. Naveen, A.R. Phani, A. Sivakumar, S.A. Martin Britto Dhas, R. Robert, Shock wave induced magnetic phase transition in cobalt ferrite nanoparticles, Mater. Chem. Phys. 275 (2022), 125300.
[56] K. Shimizu, S. Kosugi, Y. Tahara, K. Yasunaga, Y. Kaneta, N. Ishikawa, F. Hori, T. Matsui, A. Iwase, Change in magnetic properties induced by swift heavy ion irradiation in CeO_2, Nuc. Inst. Method. Phys. Res. B. 286 (2012) 291–294.
[57] H. Ohno, A. Iwase, D. Matsumura, Y. Nishihata, J. Mizuki, N. Ishikawa, Y. Baba, N. Hirao, T. Sonoda, M. Kinoshita, Study on effects of swift heavy ion irradiation in cerium dioxide using synchrotron radiation X-ray absorption spectroscopy, Nuc. Inst. Method. Phys. Res. B. 266 (2008) 3013–3017.
[58] Yue Kang, Qiang Leng, Donglin Guo, Dezhi Yang, Yanping Pu, Chenguo Hu, Room-temperature magnetism of ceria nanocubes by inductively transferring electrons to Ce atoms from nearby oxygen vacancy, Nano-Micro Lett. 8 (2016) 13–19.
[59] Nicusor Fifere, Anton Airinei, Marius Dobromir, Liviu Sacarescu, Simona I. Dunca, Revealing the effect of synthesis conditions on the structural, optical, and antibacterial properties of cerium oxide nanoparticles, Nanomaterials 11 (2021) 2596.
[60] Meenu Venugopal, S.Saravana Kumar, K.M. Nissamudeen, H. Padma Kumar, Optical and dielectric characterization of Ceria nanocrystals synthesized by an auto-igniting combustion technique, J. Mater. Sci: Mater. Electron. 27 (2016) 9496–9502.
[61] S. Tsunekawa, K. Ishikawa, Z.Q. Li, Y. Kawazoe, A. Kasuya, Origin of anomalous lattice expansion in oxide nanoparticles, Phy. Rev. Lett. 85 (2000) 3440–3443.
[62] X.D. Zhou, W. Huebner, Size-induced lattice relaxation in CeO_2 nanoparticles, Appl. Phys. Lett. 79 (2001) 3512.
[63] V. Usha, S. Kalyanaraman, R. Vettumperumala, R. Thangavel, A study of frequency dependent electrical and dielectric properties of NiO nanoparticles, Phys. B 504 (2017) 63–68.
[64] Muhammad Javed, Ayaz Arif Khan, Muhammad Nasir Khan, Jamal Kazmi, Mohd Ambri Mohamed, Investigation on non-Debye type relaxation and polaronic conduction mechanism in $ZnCr_2O_4$ ternary spinel oxide, Mater. Sci. Eng. B. 269 (2021), 115168.